Dehalogenation and coupling of a polycyclic hydrocarbon on an atomically thin insulator

Dienel, Thomas ; Gomez-Diaz, Jaime ; Seitsonen, Ari P ; Widmer, Roland ; Iannuzzi, Marcella ; Radican, Kevin ; Sachdev, Hermann ; Muellen, Klaus ; Hutter, Juerg ; Groening, Oliver

Abstract: Catalytic activity is of pivotal relevance in enabling efficient and selective synthesis processes. Recently, covalent coupling reactions catalyzed by solid metal surfaces opened the rapidly evolving field of on-surface chemical synthesis. Tailored molecular precursors in conjunction with the catalytic activity of the metal substrate allow the synthesis of novel, technologically highly relevant materials such as atomically precise graphene nanoribbons. However, the reaction path on the metal substrate remains unclear in most cases, and the intriguing question is how a specific atomic configuration between reactant and catalyst controls the reaction processes. In this study, we cover the metal substrate with a monolayer of hexagonal boron nitride (h-BN), reducing the reactivity of the metal, and gain unique access to atomistic details during the activation of a polyphenylene precursor by sequential dehalogenation and the subsequent coupling to extended oligomers. We use scanning tunneling microscopy and density functional theory to reveal a reaction site anisotropy, induced by the registry mismatch between the precursor and the nanostructured h-BN monolayer.

DOI: https://doi.org/10.1021/nn501906w

Site-selective Dehalogenation and Ullmann-type Coupling of Polycyclic Hydrocarbons on a Metal-supported Atomically Thin Insulator

Thomas Dienel[1] *, Jaime Gómez-Díaz † [2], Ari P Seitsonen[2], Roland Widmer[1], Marcella Iannuzzi[2], Kevin Radican[1], Hermann Sachdev[3], Klaus Müllen[3], Jürg Hutter[2], and Oliver Gröning[1]

[1] Empa - Swiss Federal Laboratories for Materials Science and Technology, nanotech@surfaces Laboratory, CH-8600 Dübendorf, Switzerland.

[2] University of Zurich, Department of Chemistry, Winterthurerstrasse 190, CH-8057 Zurich, Switzerland.

[3] Max Planck Institute for Polymer Research, Department of Synthetic Chemistry, Ackermannweg 10, D-55128 Mainz, Germany.

The persistent interest of chemists, physicists and material scientists in catalysis and catalytic reactions is fuelled by their pivotal relevance in enabling efficient synthesis processes. Recently, covalent coupling reactions catalysed by solid metal surfaces opened the rapidly evolving field of on-surface chemical synthesis. Using tailored molecular precursors in conjunction with the catalytic activity of the metal substrate allowed the synthesis of novel, technologically highly relevant materials like atomically precise graphene nanoribbons. However, the actual reaction site on the metal remains unclear in most cases and the intriguing question is how a specific atomic configuration between reactant and catalyst controls the reaction processes. With the reduced catalytic activity on hexagonal boron nitride (*h*-BN), the atomistic details of the sequential dehalogenation of a polyphenylene precursor, constituting the basic first step in many on-surface coupling reactions, prior to coupling to oligomers becomes accessible. Here, we use scanning tunneling microscopy (STM) and density functional theory (DFT) to study the reaction site anisotropy induced by the registry match between the precursor and the *nano*-patterned *h*-BN monolayer grown on Rh(111). The detailed understanding of the interaction between precursor molecules and substrates, as presented here, can pave the road to on-surface chemical synthesis of graphene derivatives on metal supported insulators.

An atomically thin layer of the insulating *h*-BN is a natural counterpart for graphene; matching the graphene lattice – a single layer of sp^2-hybridised carbon atoms [1] – almost perfectly with a small mismatch of approx. 2%. Currently, fabrication of these two-dimensional materials follows two main approaches: *i*) the bottom-up synthesis by substrate supported chemical vapour deposition (CVD) with suitable precursors and *ii*) the top-down approach by exfoliation. The fabrication of graphene/*h*-BN heterostructures, leading to novel devices or devices with enhanced performance, usually relies on elaborate, sequential transfer processes of the

produced layers [2]. The main obstacles in the transfer technique are possible misalignment, introduction of defects and contaminations, resulting from handling layers that are just one atom thick. Only recently, the direct CVD growth of graphene on *h*-BN was demonstrated offering superior properties [3, 4]. However, the growth conditions are harsh (long exposure time, high temperatures, several cycles, etc.) compared to the traditional CVD growth on metal substrates. Metals are favoured for their high catalytic activity, conversely bearing the disadvantage that the grown layers cannot be directly used for electronic device fabrication [5].

A common motif in catalytic reactions is the activation of a reactant, the intermittent complex formed between reactant and catalyst, and finally the coupling reaction [6]. A long-standing question in catalysis is the impact of the specific atomic configuration between catalyst and reactant on the catalytic efficiency. In other words, how does the specific atomic arrangement change the site activity and therefore influence the reaction pathways, energies and reaction yield? Thanks to the recent advances in surface science, we are witness of the tremendous progress in the understanding and development of on-surface chemical reactions and in the fabrication of nanostructured systems [6-8]. A widely used coupling reaction in this context is the Ullmann coupling [9, 10], where the reactive partners are created by dehalogenation of the precursors, which subsequently undergo the aryl-aryl coupling [11]. Recent examples are the formation of graphene nanoribbons and porous graphene on metal substrates [12-14]. The synthesis of porous graphene is based on the molecular precursor 5,5′,5′′,5′′′,5′′′′,5′′′′′-hexaiodo-cyclohexa-m-phenylene (I_6-CHP), which dissociates all its iodine atoms on Cu(111), Ag(111) and even Au(111) already at room temperature. The catalytic activity on these metals is already so high that site specific effects are difficult to study and do not seem relevant for the synthesis process. This situation can be expected to be different for a surface supported, ultra-thin insulating spacer layer like monolayer *h*-BN. The lack of electronic states close to the Fermi level will reduce the catalytic activity, whereas the ultimate thinness still allows the dehalogenation process to be studied by STM. Furthermore, the interaction between the metal and *h*-BN layer generates distinct superstructures that can be adjusted by a variation of the underlying metal (Ni [15], Pt [16], Cu [17], Rh and Ru [16, 18-24], Fe and Cr [25, 26], etc). On Rh(111) the *h*-BN forms a highly corrugated "*nanomesh*" consisting of regions with strong bonding, so-called "pores", separated by suspended "wire" regions, where the *h*-BN-Rh(111) interaction is weaker [16, 21, 24, 27-29]. Consequently, the structure of the *nanomesh* is a superposition of the 0.25 nm *h*-BN lattice and the network of pores with a lattice constant of 3.2 nm.

As we show in the following, deposition of I_6-CHP on the *nanomesh* leads to a distinct adsorption geometry imposing non-equivalency on the six iodine sites of the molecule, which is not intrinsic to the free I_6-CHP. Adsorption geometry, sequential dehalogenation and the subsequent coupling of I_x-CHP species are analysed by low-temperature scanning tunneling microscopy (LT-STM at 5.5 K) and density functional theory (DFT). Our experimental and theoretical findings show that the dehalogenation process is surprisingly strongly influenced by the substrate and shed light on the challenges of growing nanostructures by CVD routes directly on an insulating substrate, the latter being of great advantage for future applications.

Results and Discussion

The molecular petri dish. Figure 1a displays an LT-STM image with low coverage (approx. 0.15 ML) of I_6-CHP deposited onto the *nanomesh* (kept at RT during deposition). Empty pores are imaged as dark depressions [16, 21], while the adsorbed molecules have a flowerlike appearance originating from the apparent six-fold symmetric structure of a single I_6-CHP. All molecules occupy single pores and are well-separated from each other.

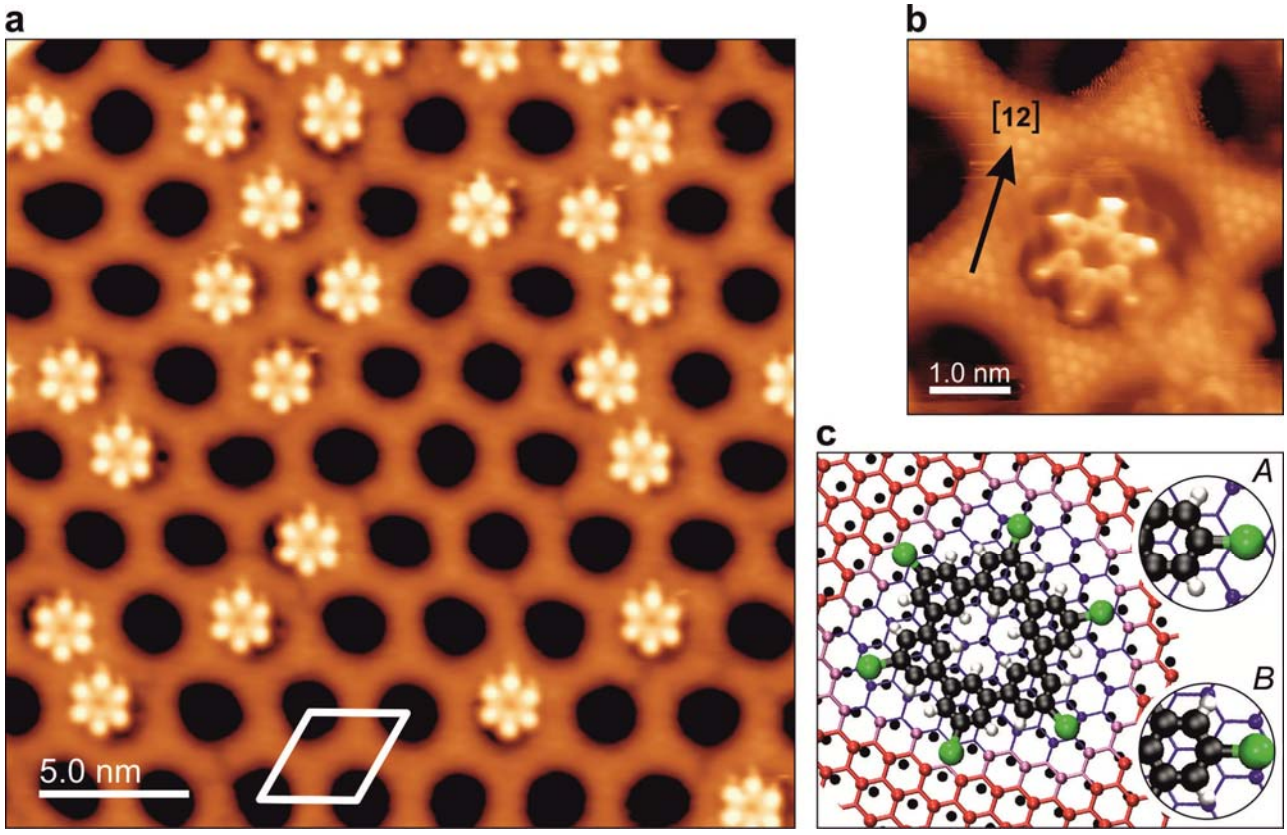

Figure 1: Molecule I_6-CHP and the *nanomesh*. **a**, STM image (-1.70 V, 40 pA) of I_6-CHP molecules occupying some of the pores of the *nanomesh* (low coverage of 0.15 ML). **b**, High resolution STM image (-1.2 V, 32 pA) of a single molecule, revealing inner contrast of the *h*-BN layer and submolecular contrast of the molecule. **c**, Ball and stick model of the DFT derived position and orientation of the I_6-CHP in the pore of the *nanomesh* (boron atoms of *h*-BN lattice enlarged; pore indicated by colour coding; black dots indicate top layer of rhodium atoms). The two insets show the different registries for the carbon-iodine bond: hollow position = *A* site; on top boron = *B* site (rhodium atoms are omitted for clarity reasons).

This is a very different situation compared to molecules on other insulating thin films typically used in STM – like alkali metal salts (NaCl, KCl, etc.) on metals. The rather homogenous structure of these dielectric spacers is of manifold advantage to study individual molecules [30-32]. However, the adsorption energy landscape for molecular species usually shows only subtle corrugation and already at low coverage (well below a closed monolayer) immediate 2-dimensional domain formation is observed, with molecular close-packing or even aggregation into 3-dimensional structures similar to single crystal insulators [33, 34]. Here on the *nanomesh*, all intermolecular distances are well defined by the lattice of the pores and are large compared to those found in close-packed I_6-CHP domains. Therefore, the intermolecular interactions between neighbouring

molecules are negligible and the species can be treated as isolated molecules, interacting solely with the substrate. Figure 1a shows the regular adsorption geometry of I_6-CHP molecules within the pores. Two major observations can be drawn immediately: i) the molecules tend to adsorb close to the rim rather than at the centre of the pore (the centre-centre distance between molecule and pore is approx. 0.4 nm) and ii) a clear preferential orientation for I_6-CHP in the pore can be observed. Within the measurement accuracy of 1° all molecules are perfectly oriented along the [12] direction of the *nanomesh*. This preferential orientation is confirmed by the DFT calculations (cf. Supplementary Information) and indicates the existence of a specific registry of the molecule and the *h*-BN lattice. While the geometry of an I_6-CHP molecule in the gas phase, as optimized by DFT, exhibits an alternating up-down tilt of the phenyl rings, this buckling diminishes on the substrate, which is consistent with STM images, where the molecules appear as planar (cf. high resolution STM imaging in Fig. 1b). The shape and size of the STM image of the molecule (outer diameter approx. 15 Å) clearly indicate that all the six iodine atoms are still covalently bonded to the aromatic macrocycle. This is in strong contrast to the case of I_6-CHP on metals, where the iodine atoms already dissociate at room temperature, leaving a sizeable space between the iodine atoms and the molecular remnant [13, 14]. The non-dissociated I_6-CHP molecules on the *nanomesh* confirm the reduced catalytic activity of *h*-BN already at the monolayer thickness on a metallic substrate. Careful analysis of atomic contrast of *h*-BN in the high resolution STM images and DFT calculations suggest that the molecules are centred above the nitrogen atoms (cf. Fig. 1c), with the I_6-CHP's carbon atoms on-top of boron or on hollow sites of the *h*-BN. This yields to two alternating, non-equivalent sites of the C-I groups with respect to the *h*-BN substrate, reducing the apparent 6-fold symmetry of the I_6-CHP to an effective 3-fold one. As shown in Fig. 1c, the *A* site is characterized by the carbon atom of the C-I group located on top of a h-BN hollow site. For the *B* site, the carbon atom is located on top of a boron atom.

Tip-induced dehalogenation of a single molecule. The circumstance that the I_6-CHP stays intact when deposited onto the *nanomesh* offers a unique opportunity to study the dissociation of its iodine atoms individually and in detail. Under appropriate tunnelling conditions, we observed low yield, spontaneous STM tip induced dehalogenation of the I_6-CHP. Figure 2 displays several stages of a typical dehalogenation sequence of a single I_6-CHP molecule, exhibiting three remarkable features: *i*) the iodine atoms dissociate at alternating positions around the molecule, *ii*) the dehalogenation comes to a halt after removing three iodine atoms and *iii*) the dissociated iodine atoms and the molecule can stay in close proximity within one pore. This is obviously an effect of the interaction with the substrate, since in the gas phase the iodine dissociation energy is the same irrespective of the iodine sites and also of the number of already dissociated iodine atoms (2 eV from a DFT calculation, cf. Supplementary Information). In other words, the free I_6-CHP molecule does not possess intrinsic site correlation with regard to the dehalogenation process. As a consequence, neither I_3-CHP species (alternating 5′,5‴,5⁗-I_3-CHP or continuous 5‴,5⁗,5⁗′-I_3-CHP) should exhibit an accentuated stability. On the *nanomesh* instead, the registry between molecule and substrate lifts the equivalency between the different iodine sites. The regularly observed case is that the iodine atoms subsequently

dissociate at positions 5′,5‴, or 5⁗ (cf. Fig. 2b to d) – which corresponds to the *B* sites of the previously assigned adsorption geometry (cf. Fig. 1c). The investigation of numerous STM tip-induced dehalogenation events shows that the sequence among the three *B* sites is random and does not involve detectable movement of the molecule.

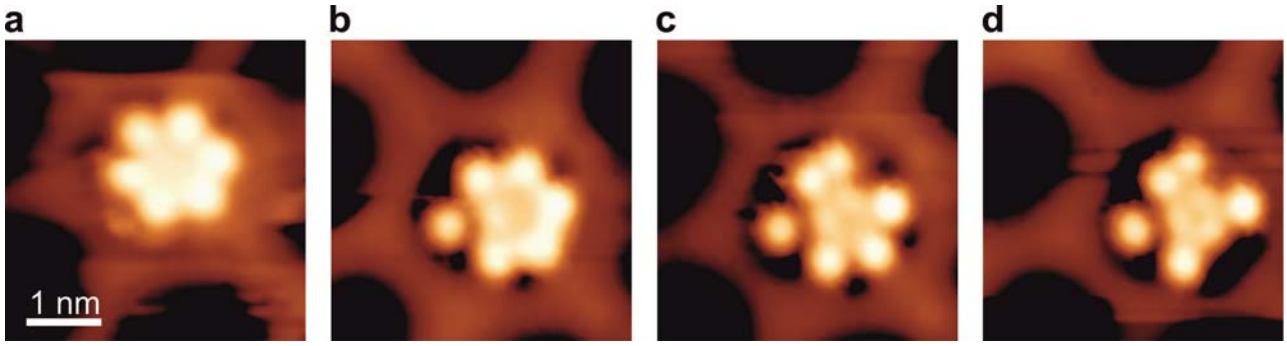

Figure 2. Sequence of **STM images during tip-induced iodine dissociation**. The continuously applied tip-sample current (1.5 V, 100 pA) during on-going STM scans leads to the dissociation of iodine atoms from I_6-CHP. Starting from an intact molecule (**a**), the iodine atoms dissociate at specific positions (the B sites: 5⁗, 5′, and 5‴ from **b** to **d**). The actual sequence is random. The highest accessible state of dissociation by this approach is the I_3-CHP (**d**). The dissociated iodine atoms can stay within the pore without affecting the molecular remnant (removal of third iodine atom in **d** does not lead to a change of the adsorption geometry). Please note the contrast change close to the centre of the molecule after removing the corresponding iodine atom.

Additionally, once the covalent iodine-carbon bond is broken, a protrusion appears close to the newly formed radical position. This effect is particularly well observed in Fig. 2b. As this protrusion is visible at STM bias voltages well within the HOMO-LUMO gap, we attribute it to a change in the conformation of the molecule rather than to an electronic effect. As we discuss later on, DFT calculations show that this conformational change is caused by a bond formation of the radical site with the underlying boron atom. Such a bond locks the molecule in position and consequently favours the remaining alternating sites for dehalogenation, *i.e.*, dissociation at all the *B* sites. However, in some rare cases the first iodine atom of I_6-CHP dissociates at an *A* site. In these cases the dehalogenation is accompanied by a small but well observable relocation of the molecule. This shift was first revealed by the DFT structure optimisation of the dehalogenated molecule and afterwards recognised in the experiments. Indeed, the shift is necessary to form the C-B bond, since the C atom is on top of a hollow site before dissociation. In this new position and consequently new registry to the substrate, the options for further dehalogenation of the molecule are limited and the opposing iodine atom is predominantly dissociated. The two bonds between molecule and substrate effectively suppress additional dehalogenations at the remaining iodine sites, *e.g.* a stable 5′,5″,5⁗,5⁗′-I_4-CHP results. Summarizing, complete dissociation at *B* sites – forming 5,5⁗,5⁗′-I_3-CHP – is by far the most commonly observed dehalogenation state and also marks the limit of tip-induced dehalogenation during continuous STM imaging. In some rare cases, we observe dehalogenation at an *A* site,

which is predominantly followed by the iodine abstraction at the opposing *B* site. In these cases the tip-induced dehalogenation stops with the formation of I_4-CHP.

Dehalogenation by thermal annealing. In order to further corroborate our findings on the orientation and site selectivity, we conducted thermally activated dehalogenation experiments. Figure 3a shows the LT-STM image after heating the sample at approx. 500 K for 15 min. A large variety of molecular species is visible, differing in the degree of dissociation (number of radical sites) and the specific position where the iodine atoms dissociated from.

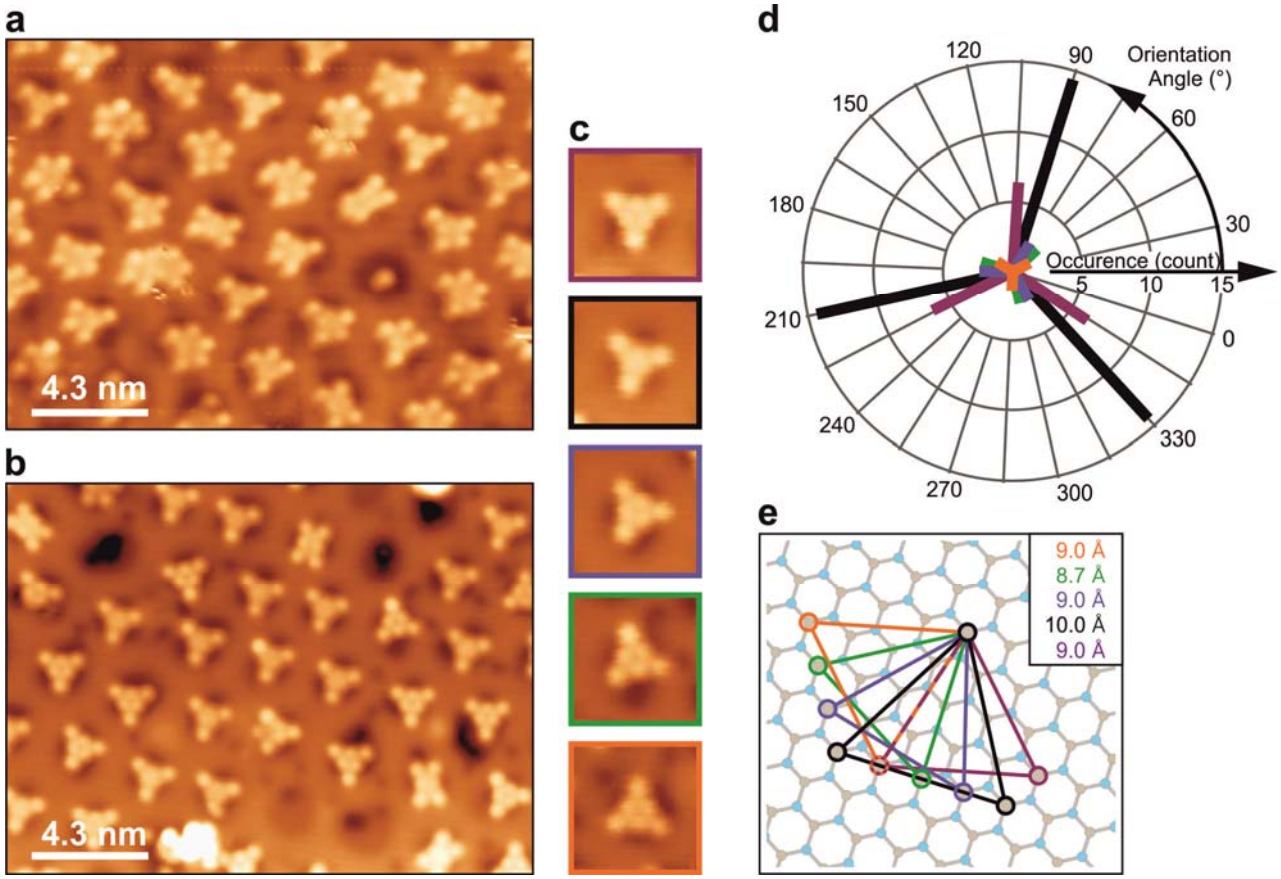

Figure 3: Iodine dissociation by thermal annealing. **a**, LT-STM image (1.2 V, 23 pA) after annealing the sample to 500 K for 15 min. Either 1, 2, or 3 iodine atoms have been dissociated per CHP molecule. Nearly all of the resulting species are oriented in the same direction, independent of the number of dissociated iodine atoms. **b**, LT-STM image (2 V, 40 pA) after treatment at 680 K for 30 min, leaving almost exclusively I_3-CHP molecules. **c**, Zoomed view of selected species of **b**, showing differently pronounced protrusions close to the centre of I_3-CHP molecules, presumably due to the formation of carbon-boron bonds after iodine dissociation. **d**, Detailed analysis of the orientations of dissociation sites in I_3-CHP in (b) relative to the lattice of the *nanomesh*. The preferred orientation is along the [12] direction (black labelled bars). **e**, Geometric correlation between an undisturbed *h*-BN lattice (lattice constant 2.5 Å) and the boron atoms presumably bonded to I_3-CHP (molecule omitted for clarity). A smaller separation between these boron atoms corresponds to a stronger tilt of the connected phenyl rings (triangles act as guides for the eye using the same colours as in (c) and (d); black for regular dissociation in [12] direction).

Unlike the tip-induced case, here the dissociated iodine can usually not be found in the pores with the molecule. They generally desorb from the surface or aggregate forming iodine islands. Despite the different stages of dehalogenation nearly all molecular species are oriented along the [12] direction of the *nanomesh*. Counting the created I_x-CHP species over a bigger field of view (cf. supplementary figure S1), more than 95% of all observed dehalogenated positions turn out to be at *B* sites of the molecule-*h*-BN registry. This motif of preferred dehalogenation sites gets even more evident when three iodine atoms dissociate, leading to the three-fold symmetric I_3-CHP with only *B* site dissociations. This circumstance nicely confirms the observation made before that the first dissociation at the I_6-CHP molecule constrains the available sites for subsequent dehalogenation steps. This preference becomes less stringent under prolonged annealing conditions at higher temperatures, where essentially I_3-CHP species are formed, but their rotational alignment within the pores is no longer limited to the exclusive [12] direction (cf. LT-STM image after thermal treatment at 680 K for 30 min. in Fig. 3b). This can be related to an increased mobility of the molecules at elevated temperatures allowing the dissociation at previously inaccessible sites on the *h*-BN lattice.

***Ab initio* simulation of dehalogenation**. To gain a deeper understanding of the unexpected site selectivity of the dehalogenation process and its persistence even at elevated temperatures, we need to answer the question, what are the atomistic processes that determine the peculiarity of the dehalogenation sites. So far we showed that the registry between molecule and substrate yields two different configurations for the iodine atoms (*A* and *B* sites) alternating on the I_6-CHP. While the DFT derived total dissociation energy for the first iodine atom from an I_6-CHP molecule on *h*-BN/Rh(111) exhibits only a small variation between *A* and *B*, the accompanying reorganization energies for the CHP remnant on the *nanomesh* vary strongly with the actual iodine site. Evaluating the dissociation process by nudged elastic band calculations shows that breaking the iodine-carbon bond is indeed accompanied by a bond formation between the unsaturated carbon atom of the iodine-free phenyl ring and the underlying boron atom of the *h*-BN (cf. distances in Supplementary Fig. S2). This bond instantly forms at *B* sites without moving the molecule (cf. Fig. 4c), while dissociation at an *A* site induces a displacement of the CHP remnant in order to let the unsaturated C atom approach the closest B atom of the substrate and form the bond (Fig. 4a). This does not only result in higher reorganization energies, *e.g.*, altered geometry of the pore, but changes the registry between the CHP remnant and the substrate. Consequently, subsequent dehalogenation steps become less favourable. Figure 4e summarizes the DFT dissociation energies for some selected sequences, where the pure *B* site dissociations (*B*-*B*-*B* in Fig. 4e) form the energetically favourable path of any triiodo-CHP final configuration. The creation of a carbon-boron bond during dehalogenation slightly lifts the boron atom, still preserving the *h*-BN integrity. The corresponding phenyl ring tilts out of the molecular plane. This geometrical change explains the small protrusion appearing in the STM images close to the centre of the CHP remnant towards the dehalogenated site (cf. Fig. 2). The lock-into-position of the molecule by the carbon-boron bond can only be counteracted by elevated annealing temperatures, leading to molecule configurations with small-angle rotation to neighbouring boron sites.

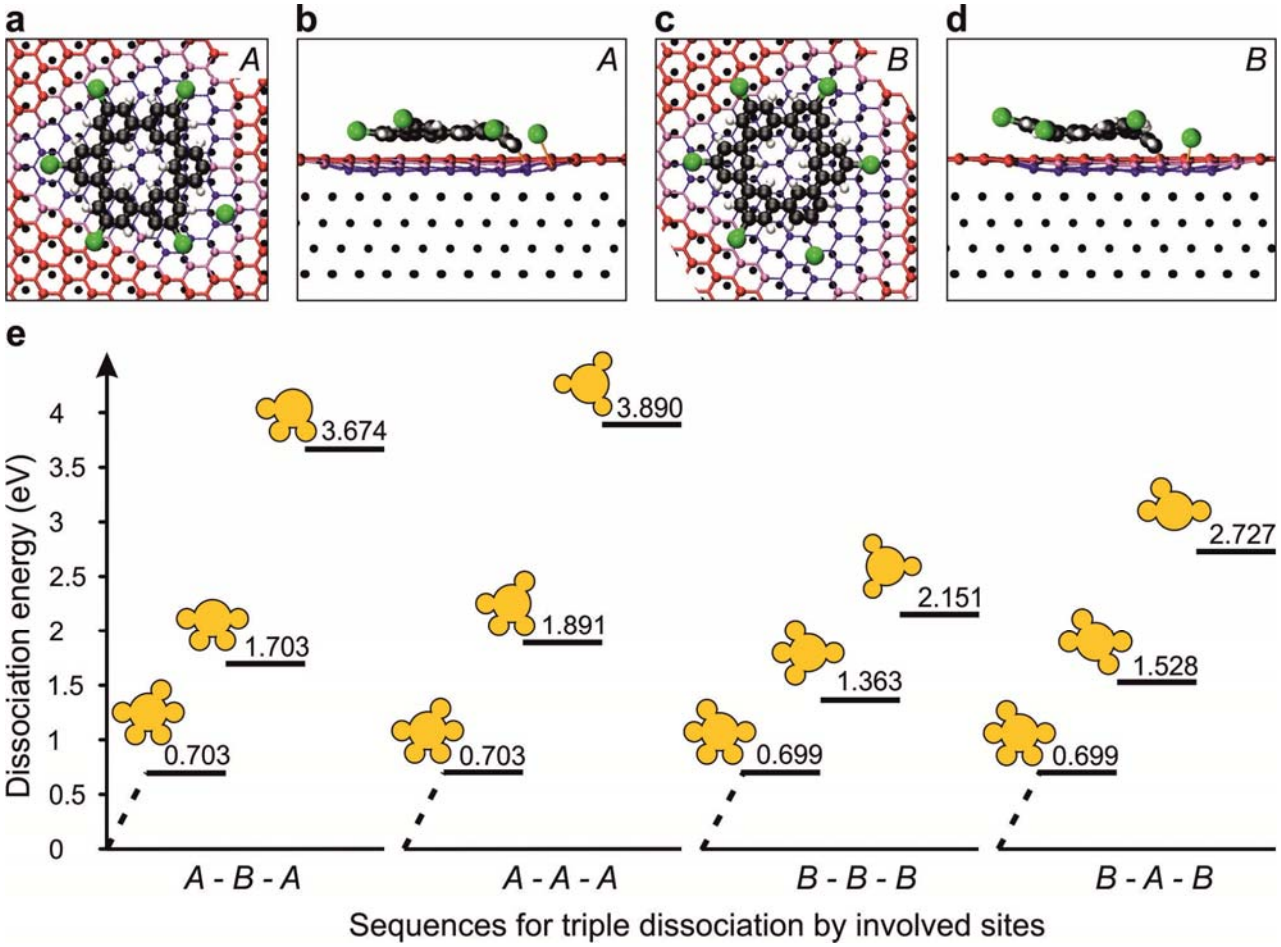

Figure 4: Dehalogenation by *ab initio* simulations. **a**, Dissociation at an *A* site resulting in a shift of the remaining molecule in the pore due to formation of a carbon-boron bond (CHP centre no longer above nitrogen atom of *h*-BN). **b**, Side view indicating a strong tilt of the corresponding phenyl rings induced by the carbon-boron bond. **c**, After a dissociation at a *B* site the molecule still at the centred at the nitrogen atom, *i.e.*, no shift of the molecule within the pore. Side view shows similar tilt of the corresponding phenyl ring (**d**). **e**, Dissociation energies of selected sequences possible during the subsequent dehalogenations of I_6-CHP on *h*-BN, starting from a fully halogenated molecule. The energies given represent the sum of dissociation energies needed to create a certain I_3-CHP species (pictograms for identification).

These orientations of the molecule, which are off the [12] direction, are however not random but correspond again to well-defined geometrical positions of the carbon radical sites bonding to boron atoms of the *h*-BN (Fig. 3c). The difference in distance between the involved boron atoms (ranging from approx. 8.7 Å to 10 Å for the different rotational states) reveals itself in a varying accentuation of the STM-topographic substructure at the position of the cyclohexa-m-phenylene macrocycle. In other words, the registry with the underlying *h*-BN lattice defines the tilting angles of the phenyl rings, as the molecular conformation must adapt itself to the shorter distance between the corresponding boron atoms. Figure 3e shows that in the cases where the boron-boron distance becomes smaller (all cases different from the [12] orientation) the protrusions are more pronounced, indicating a stronger tilt of the corresponding phenyl rings.

Oligomer formation by covalent coupling. So far, we have shown that for temperatures up to 680 K only approximately half of the iodine atoms are dissociated from I_6-CHP and the question arises whether controlled, direct aryl-aryl coupling of the Ullmann-type between two dehalogenated molecules is possible. The initially advantageous separation of single molecules in the pores of the *nanomesh* the site specific adsorption now becomes an obstacle, surmountable by a higher surface coverage of I_6-CHP molecules, i.e., decorating the wire regions of the *nanomesh*. This raises the probability that dehalogenated sites of neighbouring molecules get in sufficiently close proximity of each other and in a first step enables the formation of dimers (cf. Fig. 5a). However, the annealing temperature of 550 K leaves a significant number of covalently bonded iodine atoms, some appearing significantly brighter in STM topography. They are pushed onto the wire region of the *nanomesh* as the restricted size of a pore cannot accommodate an entire dimer. The centres of the dimers exhibit a similar substructure of bright protrusions next to the dehalogenated sites as observed for monomers, due to tilted phenyl rings, indicating the presence of carbon-boron bonds. In this context it is worth noticing that these protrusions vanish at the coupling sites, which is readily understood from the planarity of the coupling C-C bond and the absence of the C-B bonds at these positions. This effect is particularly well observed in Fig. 5a.

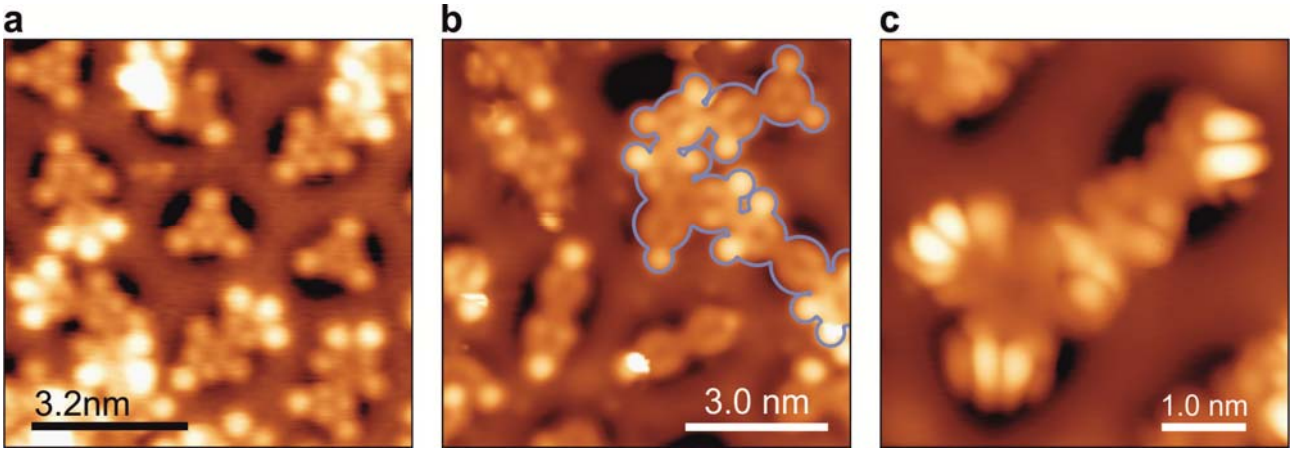

Figure 5: **Covalent coupling of CHP species at different temperatures**. **a**, STM image (-1.5 V, 30 pA) of a high coverage sample (approx. 1 ML) after treatment at 550 K for 20 min. Not only the expected I_3-CHP molecules have formed but various dimers with different iodine terminations are visible. **b**, STM image (-1.5 V, 30 pA) after treatment at 800 K for 30 min. Dimers and larger aggregates (grey outline) have formed, but despite the high temperature still contain a notable number iodine atoms. **c,** STM image (2.2 V, 20 pA) of a CHP oligomer coupled by high temperature treatment at 850 K for 30 min. The chain of coupled rings lies across two pores of the *h*-BN *nanomesh*.

Reducing the number of bonded iodine atoms and facilitating the formation of extended oligomers requires annealing temperatures above 800 K. Consequently, a large variety of species and their orientation on the *nanomesh* can be observed. In Fig. 5b, almost iodine free dimers exist alongside extended oligomers. The outlined example is comprised of 9 CHP units and spans across several unit cells of the *nanomesh*. The strong variation in appearance along the whole structure does not only originate from steric hindrance induced by the included iodine atoms, but also from bending across the wire region of the *nanomesh*. Only at annealing

temperatures of 850 K it was possible to produce iodine free oligomers as shown in Fig. 5c, where a chain of 5 connected CHP macrocycles can be seen. The fact that the structure bridges a wide area that exhibits strong variations of the surface potential [20] might contribute to the peculiar contrast in STM topography at the borders of the structure. The reason is that the locally varying surface potential can lead to an asymmetric shape of the frontier orbitals whose influence on the STM becomes important when scanning at high biases on insulating substrates [30-32].

In-depth understanding of on-surface chemical reactions between molecular species and the underlying catalytic substrate with sub-molecular resolution is vital to the synthesis of active nanostructures for organic electronics. This is particularly the case for insulating substrates, which are technologically highly relevant but have not been widely investigated in this context. With the results presented here, we can directly correlate the adsorption position of the molecule and the possibility to produce the dehalogenated species necessary for the aryl-aryl coupling. The registry and interaction between the substrate and the molecules imposes specific stable dehalogenated radical configurations. In the case of the I_6-CHP on the *h*-BN *nanomesh* this yields a large span in temperatures from the onset of dehalogenation (200°C) to full dehalogenation and coupling at (550°C). This is in strong contrast to metallic substrates like copper, silver or gold where full dehalogenation occurs already at room temperature and also to the molecule in gas phase, where the dehalogenation of the I_6-CHP is fully uncorrelated. In this respect it would be too simple to regard the effect of the *h*-BN only as an isotropic reduced catalytic activity. We have shown that the interaction of the radical with the *h*-BN substrate is highly site specific and governs the dehalogenation sequence of the molecule. This poses a challenge for the controlled coupling. The imposed site selectivity could be of use for spatially precise dissociations towards dedicated reaction pathways. This, in turn, needs the precise matching between the molecule's sites of interest and the lattice constant of the *h*-BN. This substrate itself remains quite unaffected during the reactions and only provides the required bonding sites to stabilize the intermediate molecular species prior to subsequent reactions. Finally, the Ullmann coupling – exceptionally related to metal catalysts – was demonstrated on the insulating substrate; by that pushing the door open towards the directed growth of electronic nanostructures on the intended substrate.

Methods:

All experiments were performed in a UHV apparatus (base pressure 1^{-11} mbar) comprising a low-temperature scanning tunneling microscope operated at 5.5 K (LT-STM, Omicron). The rhodium single crystal (Rh(111)) is cleaned by repeated cycles of Ar^+ ion sputtering (750 eV, grazing incidence) and thermal annealing at 1200 K. Films of h-BN were grown by thermal dehydrogenation of borazine ($(HBNH)_3$, ~50 Langmuir) on the hot metal surface (1100 K) [21, 24, 27]. This is almost self-limiting process, as the layer formation slows down once the first monolayer is completed. Subsequently, the sample is annealed at 1100 K for 15 min to promote uniform layer morphology. Software WSXM was used to analyse STM images [35]. Afterwards,

I_6-CHP molecules (see Ref. 36 for Synthesis) were deposited from a Knudsen cell, with a deposition rate of approx. 0.1 ML/min while keeping the substrate at room temperature. The PtIr-tips were cut and optimised by slight indentation during usage.

The DFT calculations were performed using the CP2K package (CP2K version 2.3.43; CP2K is freely available in http://www.cp2k.org/) with the mixed Gaussian and plane wave formalism [37] and periodic boundary conditions. The exchange and correlation functional used was the revised [38] version of the Perdew-Burke-Ernzerhof (PBE) [39] function. Long-range dispersion interactions were included using the DFT-D3 formalism [40]. The core electrons were represented by Goedecker-Teter-Hutter pseudopotentials [41]. Single- (for Rh), double- (B, N, C and I) and triple- (H and O) Zeta basis set including polarized function were employed to describe the valence electrons. The energy cutoff for the plane wave expansion representation was 500 Rydberg. The sampling in the Brillouin zone was made only at the Γ point. Due to the large size of the cell, such sampling is accurate.

The size of the cell used in the calculations is 32.1195 Å in **a** and **b** directions and 25 Å along the surface normal **c**. This corresponds to a 12x12 four layers rhodium slab with a cell parameter of 3.785 Å and an adsorbed 13x13 h-BN monolayer.

Acknowledgement: This work was supported by the SNSF (Swiss National Science Fund) under project "*Mossul*" and Sinergia project "*nanomesh*" (CRSI20-122703), CSCS (Centro Svizzero di Calcolo Scientifico) under the project s425, and the "Schrödinger" computer at University Zurich. We gratefully acknowledge helpful discussions with M. Bieri.

Contributions: T.D. and K.R. performed the STM measurements. T.D., R.W., and O.G. analysed the data and discussed the results. J.G.-D., A.P.S., M.I., and J.H. performed the DFT calculations. H.S. and K.M. provided the molecules. T.D. and A.P.S. wrote the manuscript with inputs from all other authors.

Competing financial interests: The authors declare no competing financial interests.

Corresponding author: Thomas Dienel

References:

* Corresponding author email address: thomas.dienel@empa.ch

† Jaime Gómez-Díaz: Deceased

1 **K. S. Novoselov**, V. I. Falko, L. Colombo, P. R. Gellert, M. G. Schwab, and K. Kim, *A roadmap for graphene*, Nature, 490, 192–200 (2012)

2 **L. Britnell**, R. M. Ribeiro, A. Eckmann, R. Jalil, B. D. Belle, A. Mishchenko, Y.-J. Kim, R. V. Gorbachev, T. Georgiou, S. V. Morozov, A. N. Grigorenko, A. K. Geim, C. Casiraghi, A. H. Castro Neto, and K. S. Novoselov, *Strong Light-Matter Interactions in Heterostructures of Atomically Thin Films*, Science 340 (6138), 1311-1314, (2013) doi:10.1126/science.1235547

3 **S. Roth**, F. Matsui, T. Greber, and J. Osterwalder, *Chemical Vapor Deposition and Characterization of Aligned and Incommensurate Graphene/Hexagonal Boron Nitride Heterostack on Cu(111)*, Nano Lett. 13, 2668−2675 (2013)

4 **W. Yang**, G. Chen, Z. Shi, C.-C. Liu, L. Zhang, G. Xie, M. Cheng, D. Wang, R. Yang, D. Shi, K. Watanabe, T. Taniguchi, Y. Yao, Y. Zhang, and G. Zhang, *Epitaxial growth of single-domain graphene on hexagonal boron nitride*, Nature Materials 12, 792–797, doi:10.1038/nmat3695 (2013)

5 **B. Hunt**, J. D. Sanchez-Yamagishi, A. F. Young, M. Yankowitz, B. J. LeRoy, K. Watanabe, T. Taniguchi, P. Moon, M. Koshino, P. Jarillo-Herrero, and R. C. Ashoori, *Massive Dirac Fermions and Hofstadter Butterfly in a van der Waals Heterostructure*, Science 340 (6139), 1427-1430, 2013.

6 **G. Ertl** and H. J. Freund, *Catalysis and Surface Science*, Phys. Today 52(1), 32 (1999) doi: 10.1063/1.882569

7 **G. A. Somorjai**, *Surface Science and Catalysis*, Science 227(4689), 902-908 (1985) doi: 10.1126/science.227.4689.902

8 **L. Grill**, M. Dyer, L. Lafferentz, M. Persson, M.V. Peters, and S. Hecht, *Nano-architectures by covalent assembly of molecular building blocks,* Nat. Nanotechnol. 2, 687–691 (2007)

9 **F. Ullmann** and J. Bielecki, *Ueber Synthesen in der Biphenylreihe*, Berichte der deutschen chemischen Gesellschaft 34 (2), 2174–2185 (1901)

10 **F. Ullmann**, *Ueber symmetrische Biphenylderivate*, Justus Liebigs Annalen der Chemie 332(1-2), 38–81 (1904)

11 **S.-W. Hla**, L. Bartels, G. Meyer, and K.-H. Rieder, *Inducing All Steps of a Chemical Reaction with the Scanning Tunneling Microscope Tip: Towards Single Molecule Engineering*, Phys. Rev. Lett. 85(13), 2777 (2000)

12 **J. Cai**, P. Ruffieux, R. Jaafar, M. Bieri, T. Braun, S. Blankenburg, M. Muoth, A. P. Seitsonen, M. Saleh, X. Feng, K. Müllen, and R. Fasel, *Atomically precise bottom-up fabrication of graphene nanoribbons*, Nature 466, 470–473 (2010)

13 **M. Bieri**, M. Treier, J. Cai, K. Aït-Mansour, P. Ruffieux, O. Gröning, P. Gröning, M. Kastler, R. Rieger, X. Feng, K. Müllen, and R. Fasel, *Porous graphenes: two-dimensional polymer synthesis with atomic precision*, Chem. Commun., 6919–6921 (2009)

14 **M. Bieri**, M.-T. Nguyen, O. Gröning, J. Cai, M. Treier, K. Aït-Mansour, P. Ruffieux, C. A. Pignedoli, D. Passerone, M. Kastler, K. Müllen, and R. Fasel, *Two-Dimensional Polymer Formation on Surfaces: Insight into the Roles of Precursor Mobility and Reactivity*, J. Amer. Chem. Soc. 132, 16669–16676 (2010)

15 **W. Auwärter**, M. Muntwiler, J. Osterwalder, and T. Greber, *Defect lines and two-domain structure of hexagonal boron nitride films on Ni(111),* Surf. Sci. Lett. 545, L735–L740 (2003)

16 **A. B. Preobrajenski**, A. S. Vinogradov, May Ling Ng, E. Ćavar, R. Westerström, A. Mikkelsen, E. Lundgren, and N. Mårtensson, *Influence of chemical interaction at the lattice-mismatched h-BN/Rh(111) and h-BN/Pt(111) interfaces on the overlayer morphology*, Phys. Rev. B 75, 245412 (2007)

17 **S. Joshi**, D. Ecija, R. Koitz, M. Iannuzzi, A.P. Seitsonen, J. Hutter, H. Sachdev, S. Vijayaraghavan, F. Bischoff, K. Seufert, J. V. Barth, and W. Auwärter, *Boron Nitride on Cu(111): An Electronically Corrugated Monolayer*, Nano Lett. 12(11), 5821–5828 (2012) doi: 10.1021/nl303170m

18 **M. Corso**, W. Auwärter, M. Muntwiler, A .Tamai, T. Greber, J. Osterwalder, *Boron Nitride Nanomesh*, Science 303(5655), 217-220 (2004) doi: 10.1126/science.1091979

19 **O. Bunk**, M. Corso, D. Martoccia, R. Herger, P.R. Willmott, B.D. Patterson, J. Osterwalder, J.F. van der Veen, T. Greber, *Surface X-ray diffraction study of boron-nitride nanomesh in air*, Surf. Sci. 601(2), L7-L10 (2007)

20 **H. Dil**, J. Lobo-Checa, R. Laskowski, P. Blaha, S. Berner, J. Osterwalder, and T. Greber, *Surface trapping of atoms and molecules with dipole rings*, Science 319, 1824 (2008)

21 **S. Berner**, M. Corso, R. Widmer, O. Groening, R. Laskowski, P. Blaha, K. Schwarz, A. Goriachko, H. Over, S. Gsell, M. Schreck, H. Sachdev, T. Greber, and J. Osterwalder, *Boron Nitride Nanomesh: Functionality from a Corrugated Monolayer*, Angew. Chem. Int. Ed. 46, 5115 –5119 (2007)

22 **D. Martoccia**, S. A. Pauli, T. Brugger, T. Greber, B. D. Patterson, and P. R. Willmott, h-BN on Rh(111): *Persistence of a commensurate 13-on-12 superstructure up to high temperatures*, Surf. Science 604, L9–L11 (2010)

23 **D. Martoccia**, T. Brugger, M. Björck, C. M. Schlepütz, S. A. Pauli, T. Greber, B. D. Patterson, and P. R. Willmott, *h-BN/Ru(0001) nanomesh: A 14-on-13 superstructure with 3.5 nm periodicity*, Surface Science 604, L16–L19, (2010)

24 **R. Widmer**, D. Passerone, T. Mattle, H. Sachdev, O.Gröning, *Probing the selectivity of a nanostructured surface by xenon adsorption*, Nanoscale 2, 502 (2010).

25 **N. A. Vinogradov**, A. A. Zakharov, M.L. Ng, A. Mikkelsen, E. Lundgren, N. Mårtensson, and A. B. Preobrajenski, *One-Dimensional Corrugation of the h-BN Monolayer on Fe(110)*, Langmuir 28, 1775−1781, 2012, dx.doi.org/10.1021/la2035642

26 **F. Müller**, S. Hüfner, and H. Sachdev, *One-dimensional structure of boron nitride on chromium (110) – a study of the growth of boron nitride by chemical vapour deposition of borazine*, Surf. Sci. 602, 3467–3476, 2008

27 **F. Müller**, S. Hüfner, and H. Sachdev, *Epitaxial growth of boron nitride on a Rh(111) multilayer system: Formation and fine tuning of a BN-nanomesh*, Surf. Science 603, 425–432 (2009)

28 **R. Laskowski**, P. Blaha, T. Gallauner, and K. Schwarz, Single-Layer Model of the Hexagonal Boron Nitride Nanomesh on the Rh(111) Surface, Phys. Rev. Lett. 98(10), 106802 (2007)

29 **Jaime Gomez Diaz**, Yun Ding, Ralph Koitz, Ari P. Seitsonen, Marcella Iannuzzi, and Jürg Hutter, *Hexagonal boron nitride on transition metal surfaces*, Theor. Chem. Acc. 132, 1350 (2013)

30 **J. Repp**, G. Meyer, F. E. Olsson, and M. Persson, *Controlling the Charge State of Individual Gold Adatoms*, Science 305(5683), 493-495 (2004) doi: 10.1126/science.1099557

31 **J. Repp**, G. Meyer, S. Paavilainen, F. E. Olsson, and M. Persson, *Imaging Bond Formation Between a Gold Atom and Pentacene on an Insulating Surface*, Science 312(5777) 1196-1199 (2006) doi: 10.1126/science.1126073

32 **J. Repp** and G. Meyer, *Scanning tunneling microscopy of adsorbates on insulating films. From the imaging of individual molecular orbitals to the manipulation of the charge state*, Appl. Phys. A 85(4), 399-406 (2006)

33 **T. Kunstmann**, A. Schlarb, M. Fendrich, T. Wagner, R. Möller, and R. Hoffmann, *Dynamic force microscopy study of 3,4,9,10-perylenetetracarboxylic dianhydride on KBr(001)*, Phys. Rev. B 71, 121403(R) (2005)

34 **T. Dienel**, C. Loppacher, S. C. B. Mannsfeld, R. Forker, and T. Fritz, *Growth-Mode-Induced Narrowing of Optical Spectra of an Organic Adlayer*, Adv. Mater. 20, 959–963 (2008)

35 **I. Horcas**, R. Fernández, J. M. Gómez-Rodríguez, J. Colchero, J. Gómez-Herrero, and A. M. Baro, *WSXM: A software for scanning probe microscopy and a tool for nanotechnology*, Rev. Sci. Instrum. 78, 013705 (2007)

36 **W. Pisula**, M. Kastler, C. Yang, V. Enkelmann, and K. Mullen, *Columnar Mesophase Formation of Cyclohexa-m-phenylene-Based Macrocycles*, Chem. Asian J. 2, 51-56 (2007)

37 **G. Lippert**, J. Hutter, and M. Parrinello, *A hybrid Gaussian and plane wave density functional scheme*, Mol. Phys. 92, 477-487 (1997)

38 **Y. Zhang** and W. Yang, *Comment on "Generalized gradient approximation made simple [JP Perdew, K Burke and Ernzerhof, Phys. Rev. Lett. 77, 3865–3868 (1996)]"*, Phys. Rev. Lett. 80, 890–891 (1998)

39 **J. P. Perdew**, K. Burke, and M. Ernzerhof, *Generalized gradient approximation made simple*, Phys. Rev. Lett. 77, 3865-3868 (1996)

40 **S Grimme**, J Antony, S Ehrlich and H Krieg, *A consistent and accurate ab initio parametrization of density functional dispersion correction (DFT-D) for the 94 elements H-Pu*, J. Chem. Phys. 132, 154104 (2010)

41 **S Goedecker**, M Teter and J Hutter, *Separable dual-space Gaussian pseudopotentials*, Phys. Rev. B 54, 1703-1710 (1996)

Supplementary Information for

Site-selective Dehalogenation and Ullmann-type Coupling of Polycyclic Hydrocarbons on a Metal-supported Atomically Thin Insulator

Thomas Dienel[1] *, Jaime Gómez-Díaz † [2], Ari P Seitsonen[2], Roland Widmer[1], Marcella Iannuzzi[2], Kevin Radican[1], Hermann Sachdev[3], Klaus Müllen[3], Jürg Hutter[2], and Oliver Gröning[1]

[1] Empa - Swiss Federal Laboratories for Materials Science and Technology, nanotech@surfaces Laboratory, CH-8600 Dübendorf, Switzerland.

[2] University of Zurich, Department of Chemistry, Winterthurerstrasse 190, CH-8057 Zurich, Switzerland.

[3] Max Planck Institute for Polymer Research, Department of Synthetic Chemistry, Ackermannweg 10, D-55128 Mainz, Germany.

This file includes:

Supplement text
Figures and Tables
References

DFT simulation of adsorption site. The high symmetry axis of the I_6-CHP molecule going through opposing iodine atoms is found to be aligned along the [12] direction with respect to the h-BN and the *nanomesh* lattice (cf. Supplementary Table S1a). Using this preferred orientation three lateral adsorption positions were analysed. Placing half of the carbon atoms of I_6-CHP on the boron atoms was found to be the energetically favourable position (cf. Suppl. Table S1b).

Supplementary Table S1: Adsorption energies derived by DFT. **a**) Influence of the different orientations of the CHP molecule within the pore with respect to the *nanomesh*. **b**) Variation of the adsorption position (centre of the molecule) of the CHP that is aligned in [12] direction.

a

Orientation	Adsorption energy (eV)	Relative energy (eV)
[12]	-3.810	-
[01]	-3.543	0.267
[-11]	-3.774	0.035
[-10]	-3.610	0.199

b

Position	Adsorption energy (eV)	Relative energy (eV)
C ontop B	-3.810	-
C ontop N	-3.693	0.117
C ontop both	-3.711	0.099

Dehalogenation of the free I_6-CHP by DFT. As mentioned in the main text, the inherent dehalogenation properties of a gas phase I_6-CHP molecule differ significantly from the observations made on the *nanomesh*. The DFT results in Supplementary Table S2 show that the dissociation energy is independent of the position, where the dehalogenation reaction takes place, and is also independent of the already reached dissociation

state. In other words, subsequent dehalogenation steps in a free I_6-CHP are uncorrelated. This property of the I_6-CHP in the gas phase can be understood from the distance between iodine binding sites (minimum separation = 5 carbon-carbon bonds), contrary to the situation in the much smaller hexaiodo-benzene (C_6I_6 with minimum separation given by a single carbon-carbon bond) where steric forces play a significant role for dissociation [1].

Supplementary Table S2: **Dissociation energies for the free CHP** species in the gas phase derived by DFT simulation.

	Dissociation in gas phase	Energy (eV) per step	Total Energy (eV)
1st dissociation	*position: 1*	1.991	-
2nd dissociation	*alternating: 1, 3*	1.990	*3.981*
	continuous: 1, 2	1.991	*3.982*
3rd dissociation	*alternating: 1, 3, 5*	1.991	*5.974*
	continuous: 1, 2, 3	1.993	*5.975*

Thermally assisted dehalogenation. Supplementary Figure S3 exhibits a total of 108 molecules. Excluding 22 of them with irregular shapes – e.g., additional iodine atoms, imaging artefacts, movement of molecules during scan, leaves 86 molecules that can be clearly assigned to penta-, tetra-, and triiodo-CHP. Counting the corresponding radical sites, one gets a total number of 165 dissociated iodine atoms. Only a minor amount of these iodine atoms is actually visible in the scan, indicating that a considerable number probably has desorbed from the surface during thermal treatment. The remaining iodine atoms preferentially adsorb within the pores of the *nanomesh* [2]. Of the 165 radical sites in Figure S1a, 160 are formed at *B* sites (original carbon-iodine bond on-top of boron).

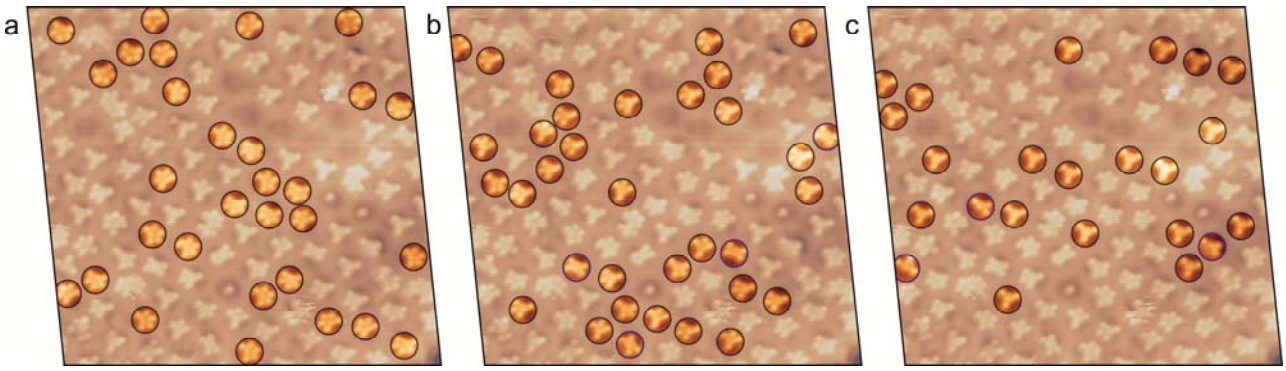

Supplementary Figure S1: Iodine dissociation by thermal annealing. STM image (1.2 V, 23 pA) after annealing with labelled species according to the number of dissociated iodine atoms from 1 to 3 (**a** to **c**). Blue encircled molecules present exceptions from the main dehalogenation scheme.

The picture becomes even clearer if we look at the doubly dehalogenated species. There we would expect three different configurations how the radical sites are distributed around a single molecule: i) neighbouring sites, ii) opposing sites, and iii) alternating sites. The first two cases by definition inherently include dissociation at *A* and *B* sites. As shown in Suppl. Fig. S1c only a small amount of I_4-CHP shows this configuration (4 out of 34). The third option exclusively requires either *A* or *B* site dissociations. Counting the corresponding species in the STM image reveals that they are all of *B* type.

The lack of dissociation events at neighbouring sites is a surprising finding if one expects a low catalytic activity and especially almost no selectivity on the *h*-BN surface. This motive of preferred dehalogenation sites becomes even more apparent when one considers that the dissociation of the third iodine atom again preferentially takes place at a *B* site again (cf. Fig. S1d). The large number of molecules in this configuration is a very surprising finding, as from a purely statistical point of view the probability to from this alternating species is 10% only, and even less by including for the specific orientation on the substrate. Instead, the experimental image exhibits a selectivity of approx. 85%.

Whereas for the majority alternate dissociation is observed, three molecules can be found with neighbouring radical sites (blue encircled molecules in Supp. Fig. S1c). This specie presumably belongs to a different dissociation path, where the first two iodine atoms are abstracted at opposing sites of the molecule.

DFT simulation of sequential dehalogenation. As discussed in the main text, the system of I_6-CHP and the *nanomesh* exhibits two different local registries of the carbon-iodine bond (*A* and *B* site). First we list some dissociation energies of some sequences leading to I_3-CHP (three dehalogenations, Supp. Table S3).

Supplementary Table S3: Dissociation energies for the stepwise dehalogenation of I_6-CHP on the *nanomesh*. The "Energy per step" is for the specific dissociation step only, while "Energy" of the whole series is the sum of the contributing steps.

	Position	Involved sites	Energy (eV) per step	Energy (eV)
1st dissociation	5	A	0.703	0.703
	5′	B	0.699	0.699
	5′′	A	0.707	0.707
	5′′′	B	0.703	0.703
	5′′′′	A	0.810	0.810
	5′′′′′	B	0.711	0.711
2nd dissociation	5, 5′′	A, A	1.188	1.891
	5′, 5′′	B, A	0.961	1.660
	5′, 5′′′	B, B	0.664	1.363
	5′, 5′′′′	B, A	0.829	1.528
3rd dissociation	5, 5′′, 5′′′′	A, A, A	1.999	3.890
	5′, 5′′′, 5′′′′′	B, B, B	0.788	2.151
	5′, 5′′′′, 5′′′	B, A, B	1.199	2.727

Nudged elastic band calculations. In order to study the reaction of iodine abstraction we performed calculations using the nudged elastic band method [3]. We employed six intermediate points; the initial and final geometries are shown in Supplementary Figure S2b and S2c, respectively. In the latter the dissociated I atom remains in the pore and binds to a B atom of the *nanomesh*. The characteristic geometrical quantities and the energy profile are shown alongside. The carbon-iodine bond labelled in Supp. Fig. S2a, is the intra-molecular bond that is broken upon dissociation, whereas the carbon-boron and iodine-boron bonds are formed once the iodine is dissociated. The reaction barrier is found to be 1.2 eV.

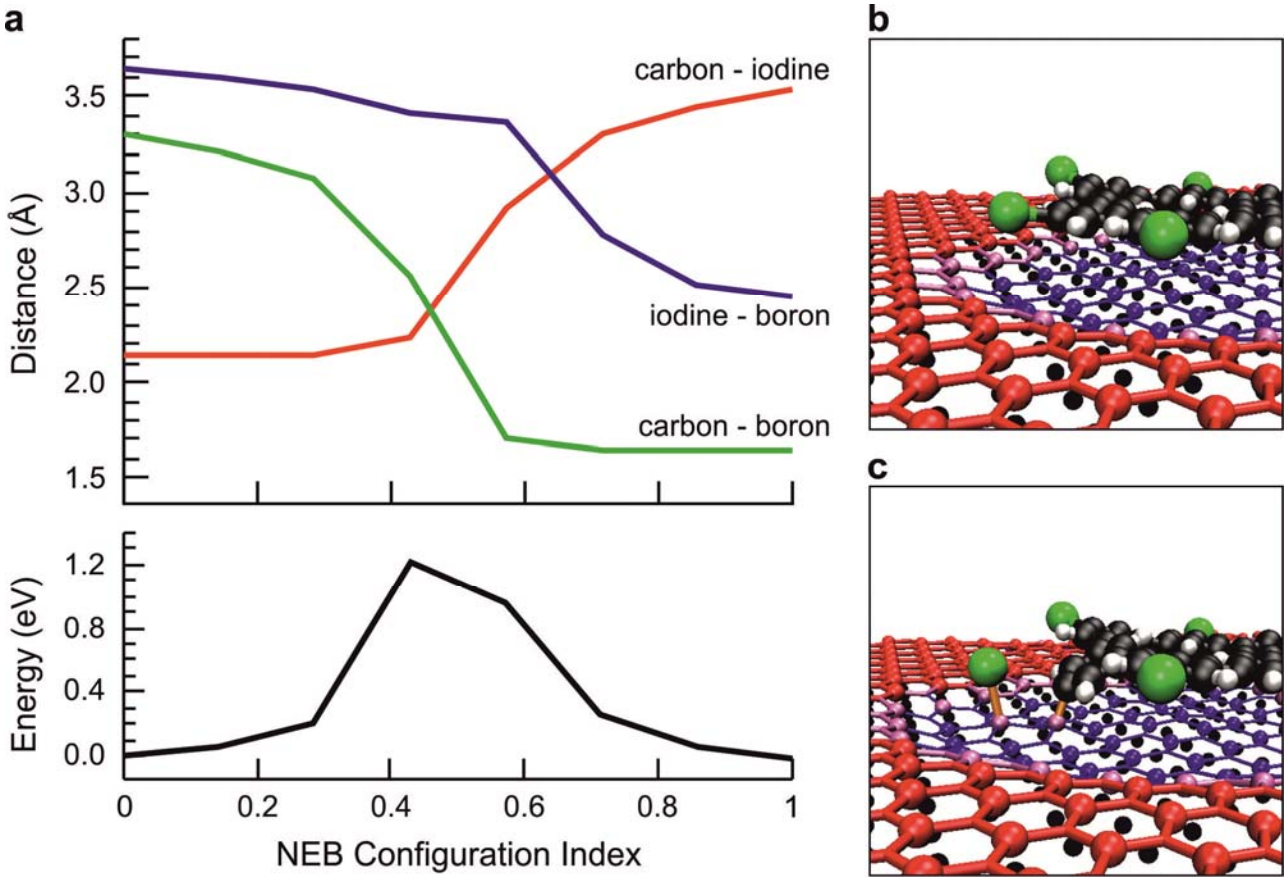

Supplementary Figure S2: Dissociation sequence for a single iodine atom calculated by the NEB method. **a**) Most relevant distances and energy during the dissociation reaction shown as function of the reaction coordinate (steps of simulation). **b**) Initial structure of an I_6-CHP molecule within the pore of the *nanomesh*, exhibiting some remaining buckling of the phenyl rings (slight up and down positions of the iodine atoms). **c**) Final structure after the dehalogenation reaction consisting of the dissociated iodine atom and the I_5-CHP remnant. The reaction leads to a strong tilt of the corresponding phenyl ring (formation of the carbon-boron bond) and deformation of the pore to accommodate the single iodine atom.

References of Supplementary Material:

1 **Jan Almloef** and Knut Faegri Jr., *Steric forces in substituted aromatics: conformation of the hexahalobenzenes as determined by ab initio calculations*, Journal of the Am. Chem. Soc. 105 (10), 2965–2969 (1983)

2 **Fabian Donat Natterer**, François Patthey, and Harald Brune, *Ring State for Single Transition Metal Atoms on Boron Nitride on Rh(111)*, Phys. Rev. Lett. 109, 066101 (2012)

3 **H. Jónsson**, G. Mills, and K. W. Jacobsen, *Nudged Elastic Band Method for Finding Minimum Energy Paths of Transitions*, in Classical and Quantum Dynamics in Condensed Phase Simulations, Ed. B. J. Berne, G. Ciccotti and D. F. Coker, 385 (World Scientific, 1998)